

## SMALL-SCALE ANISOTROPY AND INTERMITTENCE IN HIGH- AND LOW-LATITUDE SOLAR WIND

A. BIGAZZI<sup>1</sup>

Department of Electric Engineering, University of Rome Tor Vergata, Via del Politecnico, 1 00133 Rome, Italy

L. BIFERALE

Dipartimento di Fisica and INFN, Università di Roma Tor Vergata, Via della Ricerca Scientifica 1, Rome I-00133, Italy

S. M. A. GAMA

CMUP and Departamento de Matemática Aplicada, Universidade do Porto, Rua do Campo Alegre 687, 4169-007 Porto, Portugal

AND

M. VELLI<sup>2</sup>

Jet Propulsion Laboratory, California Institute of Technology, 4800 Oak Grove Drive, Pasadena, CA

Received 2004 October 29; accepted 2005 October 9

### ABSTRACT

We study low- and high-latitude fast solar wind data from the *Ulysses* spacecraft from 1992 to 1994 using for the first time a systematic method to analyze the anisotropic content of the magnetic field fluctuations beyond second-order correlation functions. We investigate all available frequencies,  $1-10^{-6}$  Hz, for both high- and low-latitude data sets in which mean magnetic field points parallel and perpendicular to the mean flow, respectively, and we are able to quantify the relative importance of the anisotropic versus the isotropic fluctuations. We analyze, up to sixth order, longitudinal, transverse, and mixed magnetic field correlations. Our results show that strongly intermittent and anisotropic events persist even at high frequencies/small scales, indicating the absence of a complete recovery of isotropy. Our study shows for the first time the existence of intermittent anisotropic contributions at all scales in solar wind. Analyses of anomalous scaling of quantities that mix isotropic and anisotropic fluctuations, like longitudinal structure functions, may therefore be flawed by systematic uncontrolled errors. Anisotropic scaling properties are compatible for high- and low-latitude data, suggesting a universal behavior in spite of the different rate of evolution of the fast solar wind streams in the two environments.

*Subject headings:* interplanetary medium — methods: data analysis — methods: statistical — solar wind — turbulence

### 1. INTRODUCTION

The solar wind is an inhomogeneous, anisotropic, and compressible magnetized plasma in which both velocity and magnetic fields fluctuate over a broad range of frequencies and scales; see, e.g., the reviews of Tu & Marsch (1995) and Horbury & Tsurutani (2001). Fluctuations may originate either from the nonlinear interactions between solar wind structures, such as the velocity streams (Coleman 1966, 1968; Matthaeus et al. 1990), or via interacting Alfvén waves produced close to the Sun and carried by the wind (Belcher & Davis 1971; Dobrowolny et al. 1980; Leamon et al. 1998). Observations of the radial evolution of magnetic fields in the inner heliosphere show the presence of fully developed turbulent spectra within a frequency range of  $10^{-4}$  to  $10^{-1}$  Hz (Bavassano et al. 1982).

The spectral index depends on the frequency range and on the distance from the Sun, varying from  $-1.2$  to  $-1.7$ . Low-frequency measurements are performed at around  $10^{-5}$  to  $10^{-2}$  Hz (Coleman 1968), while high-frequency measurements sample the range closer to  $10^{-2}$  to  $10^{-1}$  Hz (Bavassano et al. 1982; Leamon et al. 1998; Horbury & Balogh 2001). The spectral index tends to flatten closer to the Sun, indicating that turbulence is evolving in the solar wind.

Anisotropy in terms of the solar wind turbulence may mean different things: on the one hand there is the fact that the turbulence is Alfvénic; i.e., the correlation between magnetic and velocity field fluctuations in the solar wind corresponds to outwardly propagating Alfvén waves. In addition, the fluctuations in total magnetic field magnitude are small compared to the magnitude of the field fluctuations, implying that the magnetic field vector moves approximately on a sphere. Finally, there are preferred axes due to the overall solar wind expansion and the effect of solar rotation, which effectively causes the average magnetic field to become orthogonal to the radial at large distances from the Sun: this should happen preferentially at low heliomagnetic latitudes (i.e., the ecliptic plane), although a similar effect may occur even in the high-latitude heliosphere due to very low frequency transverse magnetic field fluctuations (i.e., the very low frequency part of the Alfvénic spectrum).

Phenomenological theory of hydrodynamic turbulence (Kolmogorov 1941) predicts a value of  $-5/3$  for the spectral index, while the theory of Alfvén wave-driven magnetohydrodynamic (MHD) turbulence of Iroshnikov (1963) and Kraichnan (1965) predicts a slope of  $-3/2$ . Neither prediction takes into account the possible influence of anisotropies and the presence of intermittence (Burlaga 1991, 1992; Marsch & Liu 1993; Carbone 1993; Feynman & Ruzmaikin 1994; Carbone et al. 1995b; Horbury & Balogh 1997; Ruzmaikin et al. 1995; Bruno et al. 2003; Hnat et al. 2003; Bershanskii & Sreenivasan 2004) in a systematic way.

The presence of anisotropy makes it difficult to compare observed data with the two predictions, while the presence of

<sup>1</sup> Also visiting researcher, Dipartimento di Fisica, Università di Roma Tor Vergata, Rome, Italy.

<sup>2</sup> Also at Dipartimento di Astronomia e Scienza dello Spazio, Università di Firenze, Florence, Italy.

intermittence tells us that the characteristics of the spectrum are not sufficient to characterize the system: higher order statistics need to be taken into account. In particular, spectral indices alone are insufficient to discriminate amongst turbulence models.

Anisotropy has been measured by various techniques involving the calculation of second-order moments of the field either in the real or Fourier space, such as the variance matrix or the power spectra (Belcher & Davis 1971; Carbone et al. 1995a). The eigenvector of the variance matrix corresponding to the minimum eigenvalue is usually known as the minimum variance direction. This direction is aligned with the large-scale mean field, indicating suppression of turbulence in that direction (Leamon et al. 1998; Bruno et al. 1999). Several MHD models and numerical simulations incorporate at various levels the asymmetry of the spectral indices in the field-aligned (longitudinal) and transverse directions (Shebalin et al. 1983; Zank & Matthaeus 1992; Ng & Bhattacharjee 1996; Goldreich & Sridhar 1997; Matthaeus et al. 1998; Oughton et al. 1994). Although this is a possible way to characterize anisotropy, second-order longitudinal and transverse structure functions contain both anisotropic and isotropic contributions, as is detailed in § 2. Those two contributions, always mixed, need proper treatment to be disentangled. A more systematic approach for analyzing anisotropy is therefore important. Moreover, the relation between anisotropy and intermittence has not been investigated so far.

We present in this paper a method for extracting in a systematic way, from the one-dimensional spacecraft data, information on the anisotropy and intermittence of the magnetic field fluctuations, and the interplay between them. We base our analysis on the behavior of both diagonal and nondiagonal components of higher order structure functions. We have systematically compared isotropic and anisotropic fluctuations at different scales and for different magnetic correlation functions. We measure how fast isotropy is recovered at small scales, concerning both typical fluctuations of the order of the mean standard deviation and highly intermittent events, affecting more the tails of the magnetic field probability density at all scales. We use *Ulysses* data of high-speed streams at two different points along its orbit, at high and low latitudes, in order to assess the dependence on the large-scale properties of the small-scale anisotropic fluctuations, i.e., the issue of small-scale universality.

The paper is organized as follows. In § 2 we present the set of observables needed to have a systematic control on the isotropic and anisotropic ensembles. In § 3 we present our data set and in § 4 the main results for both the low- and high-latitude data. Section 5 summarizes our findings suggesting further possible investigations.

## 2. ANISOTROPY AND STRUCTURE FUNCTION ANALYSIS

In the solar wind, as in other magnetized plasma, a strong mean magnetic field component is present. The idea of distinguishing between isotropic and anisotropic fluctuations arises naturally when one separates out the mean field component  $\mathbf{B}^0$  and the fluctuating part  $\mathbf{B}$  from the total field  $\mathbf{b}$ ,

$$\mathbf{b} = \mathbf{B}^0 + \mathbf{B}.$$

The mean field component acts as a source of anisotropy for the spatiotemporal evolution of the fluctuations. A key question is to understand how these “external” causes influence the anisotropic content of the field fluctuations at different spatial and temporal scales. The only way to do it in a systematic—controlled—way is

to decompose the field correlation functions over a suitable set of eigenfunctions that incorporate information about anisotropy. Such eigenfunctions are the eigenfunction of the group of rotation [SO(3)] and correspond to the spherical harmonics decomposition in the simple case of scalar functions.

Structure function decomposition into isotropic and anisotropic components has already been exploited with success in hydrodynamics, both for experimental and numerical data analysis (Arad et al. 1998, 1999; Kurien & Sreenivasan 2000; Biferale & Toschi 2001; Biferale & Vergassola 2001; Shen & Warhaft 2002b; see also Biferale & Procaccia 2005 for a recent review). For magnetized flows, it has been fruitfully employed in the simple case of MHD systems in which the magnetic field does not react back on the velocity, for a class of stochastic flows known as Kraichnan flows (Falkovich et al. 2001; Lanotte & Mazzino 1999; Arad et al. 2000). For both the case of pure hydrodynamics and the MHD systems described above, it has been shown that anisotropic fluctuations of the velocity and/or magnetic fields are characterized by an anomalous scaling, explaining the higher than predicted anisotropy found in the gradient statistics (Shen & Warhaft 2000, 2002a; Biferale & Vergassola 2001). It is desirable to check whether such a strong small-scale anisotropy is also found in real world magnetized plasmas such as the solar wind or if a full recovery of isotropy is observed in that case.

The way to assess the relative isotropic/anisotropic content at all scales is to perform a decomposition of the correlation functions, of order 2 and higher, over the eigenfunctions of the rotation group, as shown below. Spacecraft data are inherently one-dimensional and therefore not directly suitable for an SO(3) analysis, which requires the whole field in a three-dimensional volume, to be systematically worked out. However, we show how it is possible to extract, from the data, those correlation functions that do not contain any isotropic contribution. Their measure can be used to quantify the degree of anisotropy of the fluctuations (Kurien & Sreenivasan 2000; Staicu et al. 2003; Jacob et al. 2004).

Our data analysis is based on a set of multiscale correlation functions, built upon different combinations of magnetic field components. The most general  $n$ th-order correlation,  $S_{\alpha_1, \dots, \alpha_n}^{(n)}(\mathbf{r})$ , depending on a single separation ( $\mathbf{r}$ ), is built from the  $n$  spatial increments of magnetic field components:

$$S_{\alpha_1, \dots, \alpha_n}^{(n)}(\mathbf{r}) = \langle \delta_r B_{\alpha_1} \delta_r B_{\alpha_2} \cdots \delta_r B_{\alpha_n} \rangle, \quad (1)$$

where

$$\delta_r B_{\alpha} \equiv B_{\alpha}(\mathbf{x} + \mathbf{r}) - B_{\alpha}(\mathbf{x}) \quad (2)$$

is the difference between the values of component  $B_{\alpha}$  at two different points a distance  $\mathbf{r}$  away. Angle brackets in equation (1) indicate the average over the locations  $\mathbf{x}$ . Note that in equation (1) we have assumed homogeneity but not isotropy; i.e., the correlation functions keep their explicit dependence on the full vector  $\mathbf{r}$ . The correlation function (eq. [1]) includes both *isotropic* and *anisotropic* contributions:

$$S_{\alpha_1, \dots, \alpha_n}^{(n)}(\mathbf{r}) = S_{\alpha_1, \dots, \alpha_n}^{(n), \text{iso}}(\mathbf{r}) + S_{\alpha_1, \dots, \alpha_n}^{(n), \text{aniso}}(\mathbf{r}). \quad (3)$$

Let us remark that isotropic components are always present for any field; i.e., it is not possible to define a field that only has purely anisotropic statistical fluctuations, all projections on the isotropic sector of all correlation functions vanishing. On the other hand, fields with purely isotropic correlations do exist. We

TABLE 1  
LOW-LATITUDE AND POLAR DATA SETS

Data Set	Days	Latitude (HGL)	Distance (AU)	Speed (km s <sup>-1</sup> )	$\langle B \rangle$ (nT)
Low-latitude .....	1992 209 to 1993 137	-15 to -30	5.3-4.7	750	0.47
Polar .....	1994 245 to 265	-79.7 to -80.2	2.37-2.23	760	1.3

are therefore interested in disentangling the anisotropic and the isotropic contributions to the fluctuations. In principle, anisotropic contributions can be further classified. In this study we limit ourselves to disentangling the isotropic contribution from the anisotropic one, without entering the more subtle problem of separating out all the different anisotropies (the interested reader may consult Arad et al. [1999] and Biferale & Procaccia [2005] for a detailed illustration on how to proceed in this direction).

For  $n = 2$  and  $\alpha_1 = \alpha_2$  in equation (1), we get the well-known positively defined second-order structure function, connected to the energy spectrum  $E_{\alpha,\alpha}(\mathbf{k}) = \langle |\hat{B}_\alpha(\mathbf{k})|^2 \rangle$  via a Fourier transform. Another widely used form of equation (1) is the longitudinal structure function, obtained by projecting all field increments along the separation versor,  $\hat{\mathbf{r}}$ :  $S_r^n(r) = \langle (\delta_r \mathbf{B} \cdot \hat{\mathbf{r}})^n \rangle$ . The general form of the tensor in equation (1) for  $n = 2$  in the case of a fully isotropic and parity invariant statistics, is given by the combination of the separation vector  $\mathbf{r}$  and the only isotropic second-order tensor, the unity matrix  $\delta_{\alpha,\beta}$ :

$$S_{\alpha_1,\alpha_2}^{(2),\text{iso}}(\mathbf{r}) = \langle \delta_r B_{\alpha_1} \delta_r B_{\alpha_2} \rangle^{\text{iso}} = a(r)\delta_{\alpha_1,\alpha_2} + b(r)r_{\alpha_1}r_{\alpha_2}, \quad (4)$$

where  $a(r)$  and  $b(r)$  are two scalar functions depending only on the amplitude  $r = |\mathbf{r}|$ . Similarly, the expression for the fourth-order isotropic tensors,  $S_{\alpha_1,\dots,\alpha_4}^{(4),\text{iso}}(\mathbf{r})$ , comprises three scalar functions,  $c(r)$ ,  $d(r)$ , and  $f(r)$ :

$$\begin{aligned} S_{\alpha_1,\alpha_2,\alpha_3,\alpha_4}^{(4),\text{iso}}(\mathbf{r}) &= \langle \delta_r B_{\alpha_1} \delta_r B_{\alpha_2} \delta_r B_{\alpha_3} \delta_r B_{\alpha_4} \rangle^{\text{iso}} \\ &= f(r)r_{\alpha_1}r_{\alpha_2}r_{\alpha_3}r_{\alpha_4} + c(r)(\delta_{\alpha_1,\alpha_2}\delta_{\alpha_3,\alpha_4} + \text{perm.}) \\ &\quad + d(r)(\delta_{\alpha_1,\alpha_2}r_{\alpha_3}r_{\alpha_4} + \text{perm.}). \end{aligned} \quad (5)$$

Analogous expressions hold for higher order isotropic correlation functions. The key observation is that by a suitable choice of the combination of indices  $\alpha_1, \dots, \alpha_n$  and of the orientation  $\mathbf{r}$ , one may have the isotropic components vanish at any order  $n$  in equation (3). From now on, let us fix the separation distance in the  $\hat{\mathbf{x}}$ -direction so that  $\mathbf{r} = (r_x, 0, 0)$ . For the case  $n = 2$ , when  $\alpha_1 \neq \alpha_2$ , the resulting isotropic components vanish. We therefore have three different second-order correlation functions that are *purely anisotropic*. When the order  $n$  of the correlation function is *even*, it is enough to take an *odd* number of field increments in two different directions to have a *purely anisotropic* observable. Therefore a possible set of purely anisotropic correlations have the form

$$S_{\alpha,\beta}^{p,q}(r_x) = \langle \delta_{r_x} B_\alpha^p \delta_{r_x} B_\beta^q \rangle \quad (p + q = n), \quad (6)$$

with both  $p$  and  $q$  odd. The above  $n$ th-order correlation has a vanishing isotropic component when the combinations of indices  $\alpha = x$  and  $\beta = y, z$  are taken.

Before presenting the results of our data analysis, let us briefly comment on the translation from time series to spatial signals in our data set. Of course, as is the case for all spacecraft data, we only have access to the time evolution of the magnetic field

along the orbit. We therefore cannot make an explicit evaluation of simultaneous field increments over space. Nevertheless, the advecting velocity speed is so high (see next section for a summary of the main physical relevant quantities) that in the range of frequencies we are interested in, it is possible to safely adopt the Taylor hypothesis and translate time increments into spatial increments. The Taylor hypothesis consists of supposing the three-dimensional field as frozenly advected by the underlying large-scale velocity field,  $\mathbf{V}_0$  (Frisch 1995). Field increments in the same spatial point at two times,  $t, t'$ , are considered equal to the instantaneous field increments over two spatial locations,  $\mathbf{x}$  and  $\mathbf{x} + \mathbf{r}$ , with  $\mathbf{r} = \mathbf{V}_0(t' - t)$ . Therefore, for us, the  $\mathbf{r}$ -direction is fixed and given by the direction of the wind at the location of the spacecraft that is, within a few percent, the spacecraft-Sun direction. This direction, as noted above, we take as our reference  $\hat{\mathbf{x}}$ -axis. Spatial homogeneity is translated via the Taylor hypothesis into temporal stationarity.

### 3. ULYSSES DATA SET

The *Ulysses* orbit samples the interplanetary plasma at distances varying approximately from 1 to 6 AU, on a polar orbit. It is therefore possible to follow the evolution of plasma characteristics with distance and latitude. We use two different sets of data: the first one was taken by *Ulysses* during 1992–1993, when the spacecraft was at about 20° heliographic latitude and 5 AU distance from the Sun. The second was taken at the end of 1994, with *Ulysses* above the South Pole, at about 80° latitude and a distance of about 2 AU from the Sun. The mean field direction coincides with the radial direction in the case of the polar flows, and it is perpendicular to it, close to the  $y$ -direction, for the low-latitude data around 5 AU. This allows calculation of structure functions where the mean field lies in two different direction, parallel and perpendicular to the mean flow. This 1994 data set has just recently been made available to the community by the *Ulysses* team. Solar activity was, during the 1992–1993 period, declining, after the 1990 maximum. In 1994, the cycle was approaching the minimum of 1996. Each daily data set provides the magnitude of all three components of the interplanetary magnetic field, taken at the rate of 1 or 2 s by the Vector Helium Magnetometer on board (Balogh et al. 1992). In Table 1 we report, for the two data sets, the interval of time considered, the heliographic latitudes spanned, distance from the Sun, average speed of the wind, and average magnetic field intensity.

We preprocess data in order to clean spikes due to instrumental problems or to large shocks. This is made by excluding those data for which the jump in the magnetic field between two consecutive data points (usually 1 s apart) is larger than a threshold,  $\Delta B$ , of the order of the mean large-scale magnetic field. A fraction of data points as small as  $10^{-5}$  is discarded this way. As a result, we can access magnetic field fluctuation on a range of frequencies of almost six decades. In Table 2 we detail the total number of data points in the data set, the number of data points discarded,  $N_{\text{excl}}$ , the fraction of the latter to the total, the threshold on the maximum jump between magnetic field for

TABLE 2  
DATA SELECTION

Data Set	$N$	$N_{\text{excl}}$	$N_{\text{excl}}/N$	$\Delta B$ (nT)	$\langle B \rangle$ (nT)
Low-latitude .....	3,915,792	78	2.0E-5	0.5	0.47
High-latitude .....	1,476,051	36	2.4E-5	1.2	1.30

consecutive data points, and the average field intensity for the whole data set.

The availability of years of high-quality 1 s resolution records of data from the *Ulysses* spacecraft and the efficient algorithm for structure function calculation have made it possible to achieve such a broad range of frequencies. In fact, differently from power spectra, structure function calculations are insensitive to both nonequally spaced data and, more importantly, gaps in the data, originating either from instrumental failures or from the oscillatory character of the wind data. Thus, our algorithm calculates, for each data point and a chosen time interval  $\tau$ , the difference in the magnetic field values between time  $t_i$  and time  $t_i + \tau$ . If no data point is found at time  $t_i + \tau$ , the magnetic field is interpolated between the values at the two nearest times. This way interpolation is only performed over field values separated by the shortest sampling time (1 or 2 s, in the present case). If, instead, a gap in the data is hit at the time  $t_i + \tau$ , interpolation is only performed when gap width is less than 4 s.

### 3.1. Low-Latitude Data Set

The alternating pattern of slow and fast wind is shown in Figure 1, spanning a 10 month period, from 1992 day 209 to 1993 day 137. Within this period, we selected those sequences, of about 5 days each, when spacecraft is embedded in the trailing edges of high-speed streams and velocity is above  $650 \text{ km s}^{-1}$ . The days selected are, in 1992, 209–214, 235–241, 259–263, 337–342 and, in 1993, 28–34, 53–57, 81–85, 108–113, 133–137. They are highlighted in Figure 1 within vertical lines.

### 3.2. High-Latitude Data Set

Twenty-one consecutive days around the maximum latitude reached at perihelion, during the fast latitude scan of 1994, are

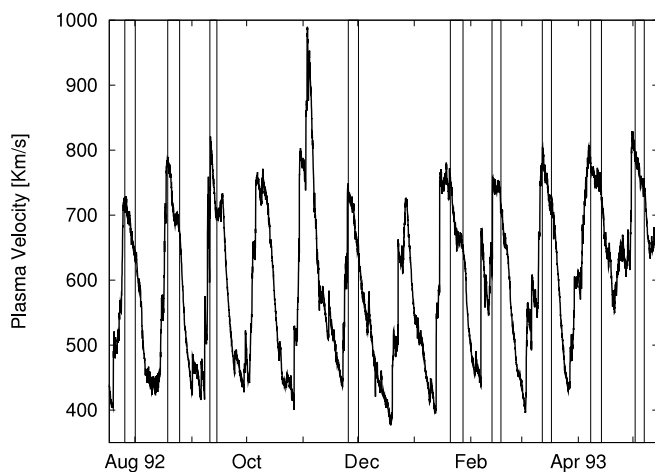


FIG. 1.—Plasma velocity sampled by the *Ulysses* spacecraft between 1992 day 209 (July 27) and 1993 day 137 (May 17). Spacecraft was between  $-15^\circ$  and  $-30^\circ$  heliographic latitude, approaching the Sun at a distance varying from 5.3 to 4.7 AU (see Table 1). Vertical lines highlight selected intervals in the trailing edges of high-speed streams.

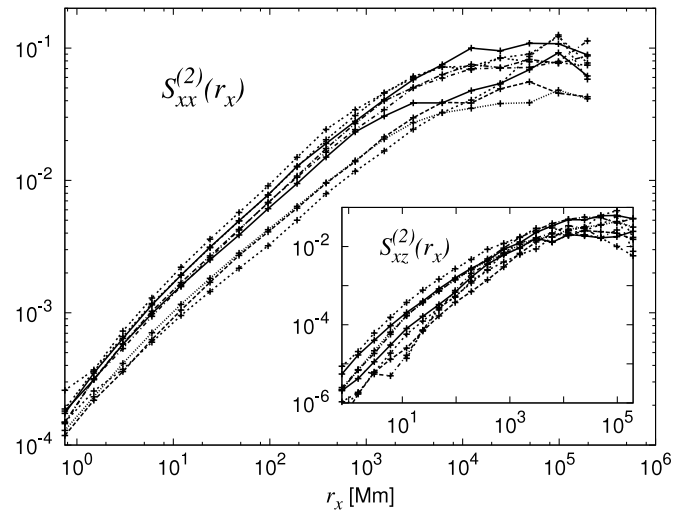


FIG. 2.—Second-order longitudinal structure function,  $S_{xx}^{(2)}(r_x)$ , for each interval comprising the low-latitude data set (see Fig. 1), as a function of the separation  $r_x$ . In the inset, the second-order purely anisotropic structure function,  $S_{xz}^{(2)}(r_x)$ .

selected. Differently from the previous data set, only the fast component of the wind is present. Table 1 lists latitude range, distance, average speed, and average magnetic field for this data set as well.

## 4. RESULTS

### 4.1. Equatorial Data

We want to first test the consistency between the disjoint sets making up the low-latitude data set of Figure 1. The second-order longitudinal structure functions, calculated for each of those intervals of contiguous data, are shown in Figure 2. They are consistent with each other over more than five decades, from 1 to  $10^5 \text{ Hz}$  in the spacecraft frame, which translates, with a mean plasma velocity of  $750 \text{ km s}^{-1}$ , into a range of  $7.5 \times 10^{-1}$  to  $7.5 \times 10^4 \text{ Mm}$ . Some intervals have a more intense signal than others do.

The anisotropic component  $S_{xz}^{(2)}$  shown in the inset of the same figure displays a similar behavior. We conclude that data from different intervals are commensurable and combine them together to obtain more stable statistical results. We refer to the combined set as the “low-latitude” data set without further distinction.

Let us now compare the undecomposed second-order structure functions with their anisotropic content. In Figure 3 we plot the longitudinal structure functions of second order,  $S_{xx}^{(2)}(r_x)$  and the two transverse structure functions in the directions perpendicular to the  $\hat{x}$ -axis,  $S_{yy}^{(2)}(r_x)$  and  $S_{zz}^{(2)}(r_x)$ . All these functions have both isotropic and anisotropic contribution:

$$S_{\alpha,\alpha}^{(2)}(r_x) = S_{\alpha,\alpha}^{(2),\text{iso}}(r_x) + S_{\alpha,\alpha}^{(2),\text{aniso}}(r_x). \quad (7)$$

The two *purely anisotropic* second-order structure functions  $S_{xy}^{(2)}(r_x)$  and  $S_{xz}^{(2)}(r_x)$  are plotted in the same figure. A few comments are in order. First, we note that the *anisotropic* correlations have a smaller amplitude with respect to the full correlation functions. This suggests that the isotropic contribution in the decomposition (eq. [3]) is dominant. Moreover, we see that the anisotropic curves decay slightly faster than the full correlation by decreasing the scale. In other words, isotropic fluctuations become more leading going to small scales, but they do so very

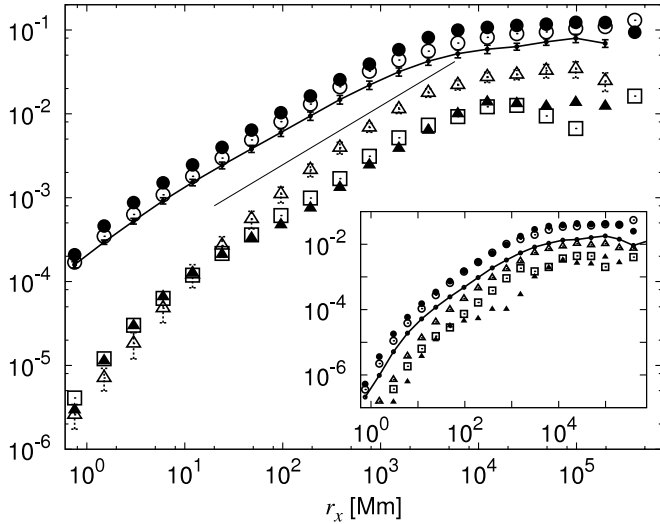


FIG. 3.—Second-order longitudinal, transverse, and *purely anisotropic* structure functions. Low-latitude data set. The top three curves show the longitudinal and transverse structure functions: solid line,  $S_{xx}^{(2)}$ ; open circles,  $S_{yy}^{(2)}$ ; filled circles,  $S_{zz}^{(2)}$ . Error bars are superimposed on  $S_{zz}^{(2)}$ . Errors are evaluated as the standard deviation of the individual intervals comprising the whole data set. The reference slope has angular coefficient of 0.7 and is shown for ease of comparison. The lower curves show the *purely anisotropic* structure functions:  $S_{xy}^{(2)}$ , filled triangles;  $S_{xz}^{(2)}$ , open triangles;  $S_{yz}^{(2)}$ , open squares. Error bars are superimposed on  $S_{xz}^{(2)}$ . Scaling exponents for the anisotropic components, indicated in Table 3, are evaluated in the range  $20-2 \times 10^3$  Mm. *Inset*: Fourth-order structure functions, longitudinal, transverse, and *purely anisotropic*. Solid line,  $S_{xx}^{(4)}$ ; open circles,  $S_{yy}^{(4)}$ ; filled circles,  $S_{zz}^{(4)}$ . *Purely anisotropic* structure functions are  $S_{xy}^{(4)}$ , filled triangles;  $S_{xz}^{(4)}$ , open triangles;  $S_{yz}^{(4)}$ , and open squares. Scaling exponents for the anisotropic components are evaluated in the range  $20-2 \times 10^3$  Mm; see Table 3.

slowly. This is consistent with the recovery-of-isotropy assumption observed in some MHD models (Lanotte & Mazzino 1999; Arad et al. 2000). We conclude that in the solar wind magnetic field becomes more and more statistically isotropic at small scales, if we limit ourselves to second-order correlation functions.

However, in order to more precisely assess this issue, it is important to control higher order statistical objects, i.e., the whole shape of the probability density distribution, at all scales. In the inset of Figure 3 we show the same comparison between longitudinal,  $S_{xxxx}^{(4)}(r_x)$ , transverse,  $S_{\alpha\alpha\alpha\alpha}^{(4)}(r_x)$  (with  $\alpha = y, z$ ), and *purely anisotropic* correlations of *fourth order* (see caption in the figure). Now the situation is quite different. First, the intensity of some *purely anisotropic* components are much closer to those with mixed isotropic and anisotropic contributions, i.e., the longitudinal and transverse structure functions. Second, the decay rate as a function of the scale is almost the same: no recovery of isotropy is detected for fluctuations of this order any more. This is the signature that anisotropy is mainly due to intense but rare events affecting high-order moments more than second-order moments. Let us note that out statistical data are quite stable, as shown by the small variations for different subsamples in Figure 2 and from the error bars estimates in Figure 3. A similar, even more pronounced, trend is observed for sixth-order quantities (not shown). The persistence of strong anisotropies at high frequencies (small scales) cast some caveat on measurements of quantities that do not properly disentangle the isotropic from the anisotropic components. As we show below when we consider the case of high-latitude data, anisotropic components have strong variations in intensity depending on the position on the solar orbit. Therefore, both latitude and distance

from the Sun influence the amount of anisotropy. As a result, undecomposed quantities that are influenced by both isotropic and anisotropic fluctuations are expected to be nonuniversal, the anisotropic content being dependent on the spacecraft position and latitude. This must hold for the spectrum and even more for higher order structure functions.

#### 4.2. Intermittence

Anisotropic fluctuations are not the unique source of complexity in solar wind data. It is well known that both magnetic and velocity fields are strongly intermittent; i.e., their statistical properties at different scales cannot be simply superimposed by rescaling. This implies the existence of anomalous scaling laws in the structure functions and “fat tails” in the PDFs of field increments (Frisch 1995). Here we want to address this issue for the first time for the anisotropic sectors. The main conclusion will be that anisotropic correlations also show anomalous scaling, their PDFs becoming more and more non-Gaussian at small scales. Moreover, anisotropic fluctuations have different overall weights at different distances and latitudes. A blind analysis of correlation functions without proper disentangling of isotropic from anisotropic contents may be flawed by systematic uncontrolled errors. In Figure 4 we show the kurtosis of both the longitudinal and transverse structure functions, i.e., the ratio between fourth-order moments and the square of the second-order moments of longitudinal and transverse increments:

$$K_{\alpha}^{(4)}(r_x) = \frac{S_{\alpha\alpha\alpha\alpha}^{(4)}(r_x)}{[S_{\alpha\alpha}^{(2)}(r_x)]^2}. \quad (8)$$

A Gaussian variable would have a kurtosis of 3, independent of the scale, while all three curves grow at small scales. We stress once more that these quantities probe both the iso- and anisotropic physics. Therefore, the scaling properties are certainly affected by the superposition of different contributions.

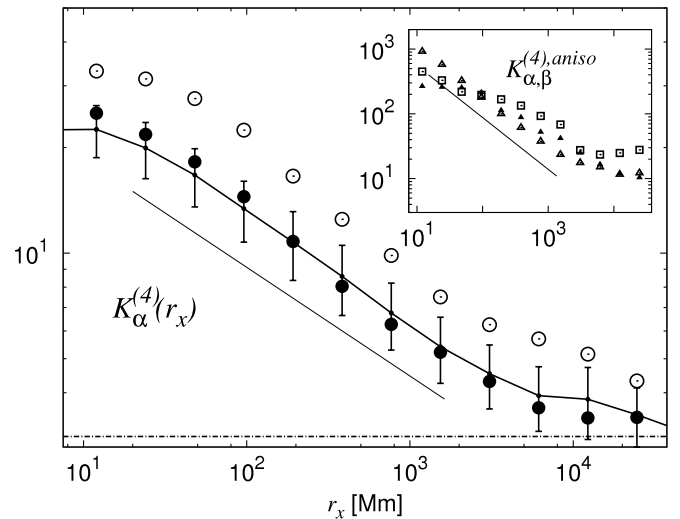


FIG. 4.—Kurtosis (eq. [8]) of longitudinal and transverse magnetic field fluctuations. Solid line,  $K_x^{(4)}(r_x)$ ; open circles,  $K_y^{(4)}(r_x)$ ; filled circles,  $K_z^{(4)}(r_x)$ . The straight line shows a linear fit in the range  $20-2 \times 10^3$  Mm, with slope  $-0.31$ , for the longitudinal component. An analogous fit for the two transverse ones returns a value of  $-0.38$ . The horizontal line corresponds to the Gaussian value of 3, attained only at large scales. *Inset*: *Purely anisotropic* kurtosis (eq. [9]).  $K_{yy}^{(4)}(r_x)$ , filled triangles;  $K_{xz}^{(4)}(r_x)$ , open triangles;  $K_{yz}^{(4)}(r_x)$ , open squares. The straight line has a slope of  $-0.8$  and represents the scaling behavior of  $\chi_4^{\text{aniso}}$  for the  $xz$  component. Scaling is evaluated in the interval  $20-2 \times 10^3$  Mm; see also Table 3. Low-latitude data set.

TABLE 3  
UNIVERSALITY: SCALING EXPONENTS (EQS. [9], [11], AND [12])

Data Set	$\zeta_2^{\text{aniso}}$	$\zeta_4^{\text{aniso}}$	$\zeta_6^{\text{aniso}}$	$\chi_4^{\text{aniso}}$	$\chi_6^{\text{aniso}}$
Low-latitude .....	$0.75 \pm 0.15$ (xy)	$0.8 \pm 0.3$ (xxxx <sup>a</sup> )	$1.2 \pm 0.4$ (xxxxyy)	$-0.6 \pm 0.2$ (xy)	$-1.2 \pm 0.3$ (xy)
	$0.95 \pm 0.10$ (xz)	$1.0 \pm 0.15$ (xzzz)	$1.2 \pm 0.2$ (xxxzzz)	$-0.8 \pm 0.2$ (xz)	$-1.5 \pm 0.3$ (xz)
	$0.75 \pm 0.10$ (yz)	$1.0 \pm 0.25$ (yzzz)	—	$-0.45 \pm 0.2$ (yz)	—
High-latitude .....	$0.75 \pm 0.15$ (xy)	$0.8 \pm 0.2$ (xxxxy <sup>a</sup> )	$1.1 \pm 0.3$ (xxxxyy)	$-0.6 \pm 0.2$ (yx <sup>a</sup> )	$-1.1 \pm 0.3$ (xy)

<sup>a</sup> Third-order contribution for these entries comes from the first component rather than from the second one, as all other cases considered.

In § 4.1 we showed that the isotropic sector is never sub-leading. We may therefore consider the above result as a confirmation that the isotropic fluctuations are indeed strongly intermittent.

Similarly, to investigate intermittence in the anisotropic sector, it is useful to define a *purely anisotropic* kurtosis, by taking the adimensional ratios of fourth-order and second-order anisotropic correlation functions:

$$K_{\alpha\beta}^{(4),\text{aniso}}(r_x) = \frac{S_{\alpha\beta\beta\beta}^{(4)}(r_x)}{[S_{\alpha\beta}^{(2)}(r_x)]^2} \sim r_x^{\chi_4^{\text{aniso}}}, \quad (9)$$

where  $\alpha$  and  $\beta$  are chosen so that contributions from the isotropic sector in both the numerator and the denominator vanish. The anisotropic components of the kurtosis (eq. [9]) are shown in the inset of Figure 4.

Functions are increasing toward small scales, with slopes of  $\chi_4^{\text{aniso}} = -0.6 \pm 0.2$ ,  $\chi_4^{\text{aniso}} = -0.8 \pm 0.2$ ,  $\chi_4^{\text{aniso}} = -0.45 \pm 0.2$  for the *xy*, *xz*, and *yz* components, respectively (see Table 3). This is the first clear indication, to our knowledge, that anisotropic fluctuations in the solar plasma are strongly intermittent. Similar trends are observed for generalized kurtosis of sixth order (not shown):

$$K_{\alpha\beta}^{(6),\text{aniso}}(r_x) = \frac{S_{\alpha\alpha\alpha\beta\beta\beta}^{(6)}(r_x)}{[S_{\alpha\beta}^{(2)}(r_x)]^3} \sim r_x^{\chi_6^{\text{aniso}}}. \quad (10)$$

There, our best estimate for the exponents is  $\chi_6^{\text{aniso}} = -1.2 \pm 0.3$ , *xy* component, and  $\chi_6^{\text{aniso}} = -1.5 \pm 0.3$ , *xz* component.

Let us here remark that the quantity in equation (9) is not constructed from ratios of fourth- and second-order moments of the same observable; i.e., it is not, rigorously speaking, the kurtosis of a stochastic variable. Nevertheless, it is a good probe of the relative intensity of fourth- versus second-order anisotropic moments, the best that can be done with a one-dimensional set of data.

A power-law fit of the numerator and denominator of equations (9) and (10) can be used to directly measure the scaling exponents of the second order,

$$S_{\alpha\beta}^{(2)}(r_x) \sim r_x^{\zeta_2^{\text{aniso}}}, \quad (11)$$

and higher order anisotropic correlation functions,

$$S_{\alpha\beta\beta\beta}^{(4)}(r_x) \sim r_x^{\zeta_4^{\text{aniso}}} \quad S_{\alpha\alpha\alpha\beta\beta\beta}^{(6)}(r_x) \sim r_x^{\zeta_6^{\text{aniso}}} \quad (12)$$

with, as customary now,  $\alpha, \beta$  are chosen in such a way that only *purely anisotropic* quantities are returned. We found  $\zeta_2^{\text{aniso}} = 0.75 \pm 0.1$  for the *xy* component,  $\zeta_2^{\text{aniso}} = 0.95 \pm 0.1$  for the *xz* component, and  $\zeta_2^{\text{aniso}} = 0.75 \pm 0.1$  for the *yz* component, see Table 3. Values for the fourth and sixth orders  $\zeta_4^{\text{aniso}}$  and  $\zeta_6^{\text{aniso}}$  may also be read out from the same table. Error bars are estimated from the maximum and minimum slopes consistent with the error bars in the range of scales from 20 to  $2 \times 10^3$  Mm. Missing entries in the table indicate that the scaling properties were not well defined within that range.

The above results show that anisotropic fluctuations, although never becoming the leading ones, are still important at small scales. Order by order, the undecomposed correlation function is more intense than any anisotropic projection. This can be visualized, for the fourth and sixth orders, by plotting the ratio between the undecomposed object and one anisotropic projection:

$$G_{xz}^{(4)}(r_x) = \frac{S_{xzzz}^{(4)}(r_x)}{S_{xxxx}^{(4)}(r_x)}; \quad G_{xz}^{(6)}(r_x) = \frac{S_{xxxzzz}^{(6)}(r_x)}{S_{xxxxxx}^{(6)}(r_x)}. \quad (13)$$

These quantities never increase at small scales, indicating that isotropic contribution in the denominator is leading with respect to the anisotropic; see Figure 5. Another quantity that can be used to characterize the relative weight of anisotropic to isotropic fluctuations, may be built from an *n*th-order anisotropic moment and the *n/2* power of a second-order isotropic moment (Shen & Warhaft 2002b; Biferale & Vergassola

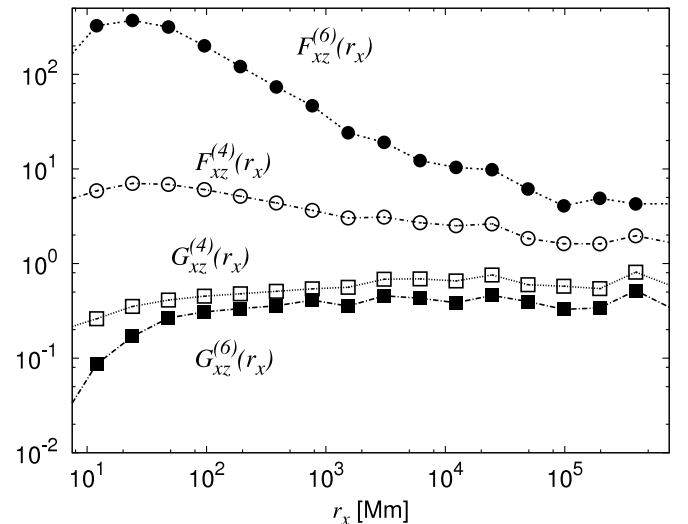


FIG. 5.—Generalized flatness  $G_{\alpha\beta}^{(n)}(r_x)$  and  $F_{\alpha\beta}^{(n)}(r_x)$  of orders 4 and 6 from eqs. (13) and (14) for components *xz* and *xy*. Low-latitude data set.

2001). For example, in our geometry, one possible choice would be

$$F_{xz}^{(4)}(r_x) = \frac{S_{xzzz}^{(4)}(r_x)}{[S_{xx}^{(2)}(r_x)]^2}, \quad F_{xz}^{(6)}(r_x) = \frac{S_{xxxxzz}^{(6)}(r_x)}{[S_{xx}^{(2)}(r_x)]^3}, \quad (14)$$

where the numerator is a *purely anisotropic*  $n$ th-order quantity, while the denominator is the second-order longitudinal structure function, raised to the  $n/2$  power. Clearly all quantities in equations (13) and (14) would be vanishing in a perfect isotropic ensemble. The difference between the two definitions (eqs. [13] and [14]) for  $F$  and  $G$  lies in the normalizing function in the denominator. In the first case,  $G$ , the normalization is through a correlation of the same order of the numerator, while in the second case,  $F$ , the normalization is via a second-order correlation raised to the appropriate power. Their amplitude as a function of  $r_x$  can be taken as a measure of the change in the anisotropic content as a function of scale. Equation (14), on the other hand, mixes correlation of different orders, thus including their possible different intermittent corrections (Biferale & Vergassola 2001). In Figure 5 we also show the behavior of  $F_{xz}^{(n)}(r_x)$  for  $n = 4, 6$ . Again, there is a clear indication of the presence of important anisotropic contributions, particularly at small scales.

We conclude this section by summarizing the main result: small-scale anisotropic fluctuations in the solar wind are dominated by intense but rare bursts, i.e., those events that influence the fourth- and sixth-order correlation functions more than second-order ones. This is particularly evident from Figure 5, where the dimensionless quantities of equation (13) are not decreasing at small scales, while quantities in equation (14) are actually increasing in the same limit.

#### 4.3. Probability Density Functions

Before concluding this section we want to rediscuss some of the previous results from the point of view of the probability density functions (PDFs). Anisotropies may be highlighted at the level of the PDF by looking at the antisymmetric part of the distribution of field increments at different scales. Let us define the PDF,  $P(X_{\alpha\beta})$ , of the dimensionless magnetic field increments at scale  $r_x$ :

$$X_{\alpha\beta}(r_x) = \frac{\delta_{r_x} B_\alpha \delta_{r_x} B_\beta}{\langle \delta_{r_x} B_x \delta_{r_x} B_x \rangle}. \quad (15)$$

In order to make the stochastic variable dimensionless we have normalized it with the longitudinal second-order structure functions at that scale. With a suitable choice of the indices  $\alpha$  and  $\beta$ , all odd moments of  $X_{\alpha\beta}(r_x)$  would be zero in a perfectly isotropic ensemble. This is the case when  $\alpha = x$  and  $\beta = y, z$ . We may now define the antisymmetric part of  $P(X_{\alpha\beta})$  as

$$A_r(X_{\alpha\beta}) = P(X_{\alpha\beta}(r_x)) - P(-X_{\alpha\beta}(r_x)), \quad (16)$$

and note that it would vanish in a symmetric isotropic ensemble.

$A_r(X_{\alpha\beta})$  gives us a direct measurement of the anisotropy as the imbalance in the probability of having oppositely directed fluctuations at that scale. In Figure 6 we show the antisymmetric part of the PDF,  $A_r(X_{\alpha\beta}(r_x))$  for  $\alpha = x$  and  $\beta = z$  for three different separations  $r_x$ . The increasingly fat tails as one goes to smaller scales reflect the non-Gaussianity of  $P(X_{xz}(r_x))$ , which becomes more enhanced at small scales. In order to assess the relative weight of the antisymmetric versus the symmetric

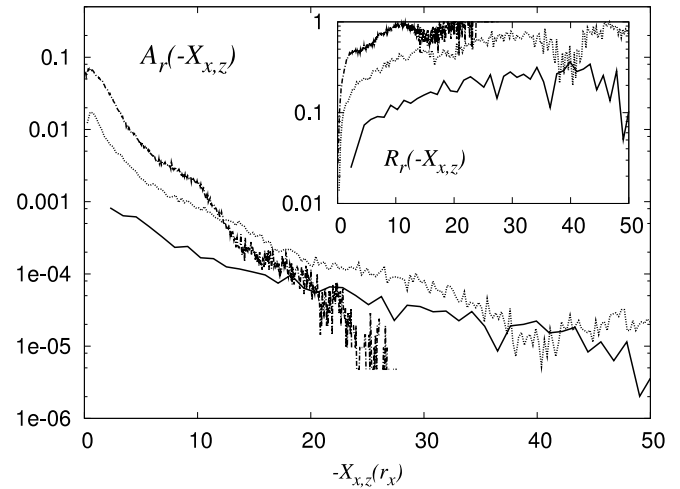


FIG. 6.—Antisymmetric part of the PDF of  $X_{xz}(r_x)$ ,  $A_r(-X_{xz})$  from eq. (16), for three different spatial separations  $r$ . Solid line:  $r = 12$  Mm, dotted line:  $r = 192$  Mm, dot-dashed line:  $r = 3072$  Mm. Inset: The normalized antisymmetric part of the PDF,  $R_r(-X_{xz})$ , from eq. (17), for the same set of  $r_x$ .

fluctuations, we define the normalized antisymmetric part of  $P(X_{\alpha\beta})$ :

$$R_x(X_{\alpha\beta}) = \frac{P(X_{\alpha\beta}(r_x)) - P(-X_{\alpha\beta}(r_x))}{P(X_{\alpha\beta}) + P(-X_{\alpha\beta})}. \quad (17)$$

This quantity also vanishes in a symmetric isotropic ensemble, approaching a value of 1 in the limit case of strong anisotropy,  $P(X_{\alpha\beta}) \gg P(-X_{\alpha\beta})$ . In the inset of the same figure,  $R(X_{xz})$  is shown. The fact that at large separations  $R(X_{xz})$  is close to one means that large events are progressively more anisotropic as they grow in intensity, a possible signature of the large-scale structures in the plasma. For small separations, the system is indeed globally more isotropic, although small-scale anisotropy never vanishes and survives at a significant level of 10% for all intensities.

#### 4.4. High-Latitude Data

We discuss here anisotropy and intermittence detected in the polar region by *Ulysses*. This allows us to address the “universality” of anisotropy, i.e., to quantify to what extent intensities of anisotropic fluctuations and their scaling properties are dependent/independent on the mean large-scale structure on the magnetized plasma. There are two effects that might influence the relative anisotropy of the turbulence in the polar and equatorial regions. In the polar regions, the amplitude of turbulence relative to the mean field is stronger, while the effects of solar rotation, which tend to bend the interplanetary magnetic field into a spiral, are negligible. In the equatorial high-speed streams, the average magnetic field is bent into the Parker (spiral) direction, so that there are two main axes that may influence the evolution of the fluctuations, the radial and the mean field directions. We remind the reader that the mean field direction coincides with the radial direction for polar flows, while it is perpendicular to it, close to the  $y$ -direction, for the low-latitude data around 5 AU.

Let us first present results on the overall relative importance of anisotropic fluctuation with respect to the undecomposed ones. In Figure 7 we show the same as in Figure 3 but for polar data. *Purely anisotropic* structure functions have a much lower intensity (1 order of magnitude less) with respect to the longitudinal

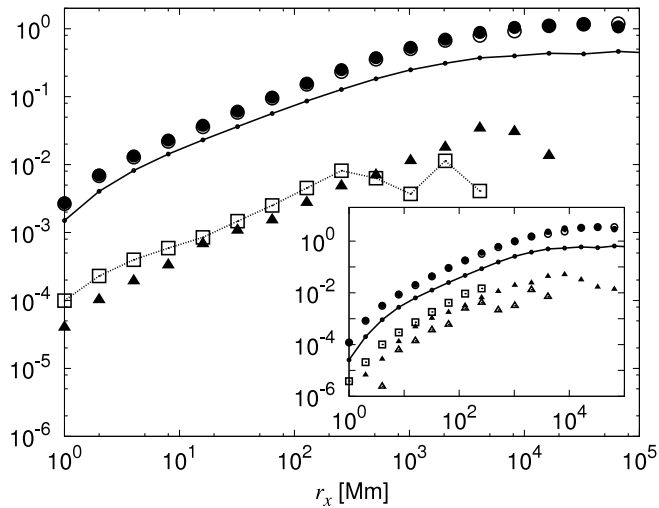


FIG. 7.—Same as in Fig. 3, but for the polar data set. Second-order longitudinal, transverse, and *purely anisotropic* structure functions. The top three curves show the longitudinal and transverse structure functions: solid line,  $S_{xx}^{(2)}$ , open circles,  $S_{yy}^{(2)}$  and filled circles,  $S_{zz}^{(2)}$ . The lower curves show the purely anisotropic structure functions:  $S_{yy}^{(2)}$ , filled triangles;  $S_{zz}^{(2)}$ , open squares. The scaling behavior for the anisotropic component  $S_{yy}^{(2)}$  is evaluated in the interval  $20-2 \times 10^3$  Mm, see also Table 3. *Inset*: Fourth-order structure functions, longitudinal, transverse and *purely anisotropic*. Solid line,  $S_{xxxx}^{(4)}$ , open circles,  $S_{yyyy}^{(4)}$ , filled circles,  $S_{zzzz}^{(4)}$ . *Purely anisotropic* structure functions are  $S_{yyyy}^{(4)}$ , filled triangles;  $S_{zzzz}^{(4)}$ , open triangles;  $S_{xyyy}^{(4)}$ , open squares. The scaling for  $S_{xyyy}^{(4)}$  is evaluated in the interval  $20-2 \times 10^3$  Mm.

and transverse structure functions both for the second order (body of the figure) and for the fourth order (inset). Indeed, for higher order moments, 6 and higher, the statistical fluctuations combined with the very low intensity of the anisotropic signal do not allow stable results even with the whole statistic of 21 consecutive days we analyzed. We conclude therefore that the anisotropy content at this latitude is much lower than in the low-latitude data set. One could argue that at this latitude averaging over long periods may hide important physical phenomena that appear on a shorter time window. Therefore, we also selected periods of 2–3 consecutive days when the anisotropic signal looked more stable and intense. The anisotropic content in those events is slightly more important and allows us to make a quantitative estimate of its scaling properties, but do not differ qualitatively.

In Figure 8 we show the same as Figure 4, for the polar data set. We show the kurtosis of longitudinal and transverse magnetic field fluctuations together with the kurtosis for *purely anisotropic* correlation functions (eq. [9]). Comparing the scaling behaviors of all the statistical indicators considered, summarized in Table 3, we have a qualitative agreement between the high-latitude and the low-latitude data sets. If confirmed by other measurements, and/or with higher statistical data sets, this would be a nice indication of “universality” in the small-scale fluctuations of the solar wind plasma. Overall intensities of isotropic and anisotropic contents are of course dependent on the distance and latitude, while their variation with scale/frequency look more stable.

## 5. CONCLUSIONS

Our main finding is that strong anisotropic fluctuations persist at all scales in the fast solar wind. In the equatorial region, the anisotropic contents of the fourth-order correlation function is roughly of the same order as its isotropic part, at all scales, indicating that small-scale isotropy is never achieved. Also, a high degree of intermittence is measured in purely anisotropic fluctuations. In the polar region, anisotropies are smaller and

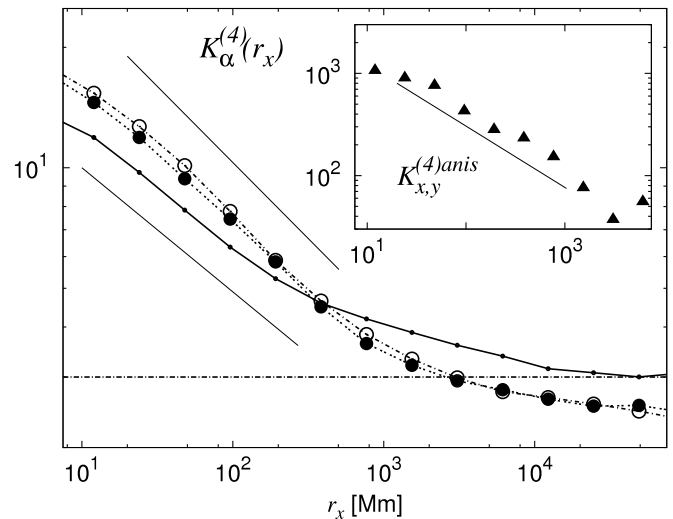


FIG. 8.—Same as in Fig. 4. Polar data set. Kurtosis (eq. [8]) of the longitudinal and transverse magnetic field fluctuations. Solid line,  $K_\alpha^{(4)}(r_x)$ , open circles,  $K_y^{(4)}(r_x)$ , and filled circles,  $K_z^{(4)}(r_x)$ . The dot-dashed line shows the constant level of three for the kurtosis of a Gaussian variable. *Inset*: *Purely anisotropic* kurtosis (eq. [9]) of component  $K_{yy}^{(4)}(r_x)$  (triangles). Its scaling exponent is evaluated in the interval  $20-2 \times 10^3$  Mm; see also Table 3.

highly fluctuating in time, but with a spatial dependence compatible, within statistical errors, with the one observed at low latitudes.

This would indicate some universal features of anisotropic solar fluctuations independently of the latitude, at least for what concerns their scaling properties. Our results point toward a crucial role played by anisotropic fluctuations in the small-scale statistics. This poses a question to many previous studies focusing on the anomalous scaling of quantities that mix isotropic and anisotropic fluctuations such as longitudinal structure functions. In particular, for equatorial solar wind, where anisotropic fluctuations are more important, our study shows that a blind analysis of structure functions may be flawed by out of control contributions. The implications of our results for the dynamics of the dissipative structures in solar wind turbulence remain to be investigated. We showed that both anisotropy and intermittence are important at small scales. Unfortunately, *Ulysses* data do not allow dissipative structures to be resolved, as the higher data sampling frequency lies just at the verge of the inertial range.

A tentative explanation of the differences between high and low latitudes may be sketched as follows: Close to the equator, two distinct preferential directions exist, the radial one and the Parker spiral direction. A linearly propagating Alfvén wave is characterized by a wave-vector  $k$ , which tends to align with the radial direction. Its natural polarization direction therefore tends to be orthogonal to the ecliptic. In polar regions, instead, the only direction singled out is the radial one. Low-frequency magnetic field fluctuations should show a preferential transverse direction, but given the invariance under rotation around the radial direction, the result is a strong fluctuating anisotropy whose average is much smaller than in the previous situation.

Bruno et al. (1999) showed that by removing small-scale discontinuities in the data set, the Iroshnikov Kraichnan phenomenology is recovered. It would be of interest to confirm or extend their results on other data sets with the help of the tools we have presented in this paper. Also, it would be interesting to recast the Goldreich & Sridhar (1997) theory in the framework presented here, in order to get a phenomenological prediction on the behavior of anisotropic fluctuations, independently of the

presence of intermittence. Models in which higher order statistic is also taken into account, providing estimates for the scaling exponents of higher order anisotropic structure functions, will be important to a deeper understanding of solar wind turbulence. Anisotropy and intermittence may also be important in the context of scattering of particles in the heliosphere (see, e.g., Giacalone & Jokipii 1996) Before concluding, let us go back to the issue of distinguishing different anisotropic fluctuations.

As we mentioned in § 1, the exact decomposition in different anisotropic sectors is possible only using numerical data, where the full magnetic field, in a finite portion of the three-dimensional space, is available. In this paper, we have described the procedure that should be adopted for one-dimensional strings of data. For those data “whole” anisotropic components can be extracted. However, there is not a unique “anisotropic” sector; rather, different anisotropic properties are described by projection on the eigenfunctions with different total angular momentum,  $j$ , and

projections of the total angular momentum on a given axis,  $m$  (Arad et al. 1999). This implies that all estimates of the scaling properties reported here may be affected by out-of-control contributions from different anisotropic sectors. If, of all anisotropic sectors, only the leading one is dominating the statistics at small scales, then our results hold the dominant contribution. This hypothesis implies a hierarchy between the scaling exponents in different sector and has been verified on direct numerical simulations of turbulent flows (Biferale & Toschi 2001; Biferale et al. 2002) and on analytical calculation for passive magnetic fields (Lanotte & Mazzino 1999; Arad et al. 2000), but it remains an open question for active magnetic fields.

We thank B. Bavassano, R. Bruno, A. Lanotte, and F. Toschi for fruitful discussions. We acknowledge support from EU under the grant “Nonideal Turbulence” HPRN-CT-2000-0162.

## REFERENCES

- Arad, I., Biferale, L., & Procaccia, I. 2000, *Phys. Rev. E*, 61, 2654  
 Arad, I., Dhruva, B., Kurien, S., L'vov, S.V., Procaccia, I., & Sreenivasan, K. R. 1998, *Phys. Rev. Lett.*, 81, 5330  
 Arad, I., L'vov, V., & Procaccia, I. 1999, *Phys. Rev. E*, 59, 6753  
 Balogh, A., Beek, T. J., Forsyth, R. J., Hedgecock, P. C., Marquedant, R. J., Smith, E. J., Southwood, D. J., & Tsurutani, B. T. 1992, *A&AS*, 92, 221  
 Bavassano, B., Dobrowolny, M., Mariani, F., & Ness, N. F. 1982, *J. Geophys. Res.*, 87, 3617  
 Belcher, J. W., & Davis, L. J. 1971, *J. Geophys. Res.*, 76, 3534  
 Bershadskii, A., & Sreenivasan, K. R. 2004, *Phys. Rev. Lett.*, 93, 064501  
 Biferale, L., Daumont, I., Lanotte, A., & Toschi, F. 2002, *Phys. Rev. E*, 66, 056306  
 Biferale, L., & Procaccia, I. 2005, *Phys. Rep.* 414, 43  
 Biferale, L., & Toschi, F. 2001, *Phys. Rev. Lett.*, 86, 4831  
 Biferale, L., & Vergassola, M. 2001, *Phys. Fluids*, 13, 2139  
 Bruno, R., Bavassano, B., Pietropaolo, E., Carbone, V., & Veltri, P. 1999, *Geophys. Res. Lett.*, 26, 3185  
 Bruno, R., Carbone, V., Sorriso-Valvo, L., & Bavassano, B. 2003, *J. Geophys. Res.*, 108, 8  
 Burlaga, L. F. 1991, *J. Geophys. Res.*, 96, 5847  
 ———. 1992, *J. Geophys. Res.*, 97, 4283  
 Carbone, V. 1993, *Phys. Rev. Lett.*, 71, 1546  
 Carbone, V., Malara, F., & Veltri, P. 1995a, *J. Geophys. Res.*, 100, 1763  
 Carbone, V., Veltri, P., & Bruno, R. 1995b, *Phys. Rev. Lett.*, 75, 3110  
 Coleman, P. J. 1966, *J. Geophys. Res.*, 71, 5509  
 ———. 1968, *ApJ*, 153, 371  
 Dobrowolny, M., Mangeney, A., & Veltri, P. 1980, *Phys. Rev. Lett.*, 45, 144  
 Falkovich, G., Gawędzki, K., & Vergassola, M. 2001, *Rev. Mod. Phys.*, 73, 913  
 Feynman, J., & Ruzmaikin, A. 1994, *J. Geophys. Res.*, 99, 17645  
 Frisch, U. 1995, *Turbulence: The legacy of A. N. Kolmogorov* (Cambridge: Cambridge Univ. Press)  
 Giacalone, J., & Jokipii, J. R. 1996, *J. Geophys. Res.*, 101, 11095  
 Goldreich, P., & Sridhar, S. 1997, *ApJ*, 485, 680  
 Hnat, B., Chapman, S. C., & Rowlands, G. 2003, *Phys. Rev. E*, 67, 056404  
 Horbury, T. S., & Balogh, A. 1997, *Nonlinear Processes Geophys.*, 4, 185  
 ———. 2001, *J. Geophys. Res.*, 106, 15929  
 Horbury, T. S., & Tsurutani, B. 2001, in *The Heliosphere Near Solar Minimum: The Ulysses Perspective*, ed. A. Balogh, R. G. Marsden, & E. J. Smith (London: Springer), 167  
 Iroshnikov, P. S. 1963, *AZh*, 40, 742  
 Jacob, B., Biferale, L., Iuso, G., & Casciola, C. M. 2004, *Phys. Fluids*, 16, 4135  
 Klein, L.W., Bruno, R., & Bavassano, B. 1993, *J. Geophys. Res.*, 98, 17461  
 Kolmogorov, A. N. 1941, *Dokl. Akad. Nauk SSSR*, 30, 301 (Eng. transl. in *Proc. R. Soc. Lond. A*, 434, 9 [1991])  
 Kraichnan, R. H. 1965, *Phys. Fluids*, 8, 1385  
 Kurien S., & Sreenivasan, K. R. 2000, *Phys. Rev. E*, 62, 2206  
 Lanotte, A., & Mazzino, A. 1999, *Phys. Rev. E*, 60, 3483  
 Leamon, R. J., Smith, C. W., Ness, N. F., Matthaeus, W. H., & Wong, H. K. 1998, *J. Geophys. Res.*, 103, 4775  
 Marsch, E., & Liu, S. 1993, *Ann. Geophys.*, 11, 227  
 Matthaeus, W. H., Goldstein, M. L., & Roberts, D. A. 1990, *J. Geophys. Res.*, 95, 20673  
 Matthaeus, W. H., Oughton, S., Ghosh, S., & Hossain, M. 1998, *Phys. Rev. Lett.*, 81, 2056  
 Ng, C. S., & Bhattacharjee, A. 1996, *ApJ*, 465, 845  
 Oughton, S., Priest, E. R., & Matthaeus, W. H. 1994, *J. Fluid Mec.*, 280, 95  
 Ruzmaikin, A. A., Feynman, J., Goldstein, B. E., Smith, E. J., & Balogh, A. 1995, *J. Geophys. Res.*, 100, 3395  
 Shebalin, J. V., Matthaeus, W. H., & Montgomery, D. 1983, *J. Plasma Phys.* 29, 525  
 Shen, X., & Warhaft, Z. 2000, *Phys. Fluids* 12, 2976  
 ———. 2002a, *Phys. Fluids*, 14, 370  
 ———. 2002b, *Phys. Fluids*, 14, 2432  
 Staicu, A., Vorselaars, B., & van de Water, W. 2003, *Phys. Rev. E*, 68, 046303  
 Tu, C.-Y., & Marsch, E. 1995, *Space Sci. Rev.*, 73, 1  
 Zank, G. P., & Matthaeus, W. H. 1992, *J. Geophys. Res.*, 97, 17189